Catalysis Today 178 (2011) 164–171

Contents lists available at SciVerse ScienceDirect

Catalysis Today

journal homepage: www.elsevier.com/locate/cattod

# Designing nanoscopic, fluxional bimetallic Pt–Ru alloy hydrogenation catalysts for improved sulfur tolerance

Jessica N.G. Stanley, Katy Worthington, Falk Heinroth, Anthony F. Masters, Thomas Maschmeyer*

*Laboratory of Advanced Catalysis for Sustainability, School of Chemistry, F11 The University of Sydney, Sydney, NSW 2006, Australia*

ARTICLE INFO

*Article history:*
Received 2 June 2011
Received in revised form 16 August 2011
Accepted 1 September 2011
Available online 5 October 2011

Dedicated to the memory of David Trimm, an esteemed colleague and valued friend.

*Keywords:*
Catalysis
Metal nanoparticles
Sulfur poisoning

ABSTRACT

Supported Pt and Ru mono- and bimetallic alloy catalysts, with promising potential applications in biomass processing, were investigated for their tolerance to sulfur poisoning using the batch hydrogenation of cyclohexene to cyclohexane in the presence of thiophene as a screening reaction. Compared to their monometallic counterparts, the bimetallic catalysts exhibited higher turnover frequencies, both in the absence and presence of sulfur. XRD analysis of changes in the Pt unit cell size suggest that the observed restructuring of the metal nanoparticles results from increasing amounts of sulfur species being coordinated to the ruthenium during poisoning, leading to at least a partial separation of the alloy. However, regeneration of the catalyst in pure $H_2$ at 300 °C shows this to be a reversible process. The sulfur tolerance observed for catalysts with certain Ru to Pt ratios might be due to sulfur and hydrogen intra-particle spillover.



## 1. Introduction

The finite nature of our fossil fuel reserves, combined with increasing environmental concerns related to emissions from fossil fuel combustion, make it ever more important to find sustainable and environmentally-friendly energy sources. In particular, supplies of liquid transport fuels (petrol, diesel, jet fuel) will be dwindling rapidly in the next forty years [1]. Biomass is an attractive alternative source of liquid transport fuels, as it is the only foreseeable source of sustainable liquid fuels and chemicals [1–5], and is more evenly distributed geographically than are fossil fuel reserves [6]. However, as biomass-based feedstocks have a high oxygen and moisture content, lower thermal stabilities, and higher degrees of functionality than do petroleum feedstocks, new chemical pathways and catalysts are required for biomass processing [7]. The current "in-principle" approaches for the conversion of lignocellulosic biomass to liquid fuels include gasification (followed by Fischer-Tropsch chemistry) [2,8], pyrolysis [9,10], hydrothermal liquefaction [11,12], delignification (pulping) followed by saccharification and fermentation [7,13], and aqueous phase reforming (APR) [1,14]. Supported metal catalysts play an important role in many of these processes. For example, the gasification of biomass in supercritical water is improved by metal catalysts [15–20], and Rioche et al., continuing studies by Chornet et al. on the steam reforming of bio-oil over Ni-based catalysts [21–26], found that ceria–zirconia supported noble metal catalysts were more efficient than alumina supported catalysts [10]. Recently, Dumesic et al. reported that biomass-derived feedstocks can be converted to hydrogen [27–33], and to gaseous [31,34,35], and liquid [36–41] alkanes using supported metal catalysts, and that the processes can be tailored to produce alkanes rather than hydrogen by tuning the catalyst and $H_2$/CO concentrations in the reactor.

However, it is expected that the presence in real biomass feedstocks of sulfur (present in amino acids such as cysteine and methionine, and resulting from the uptake of soil nutrients) with values ranging from 10 ppm to 1000 ppm [42] will significantly impair catalytic performance, and thus there is a great need to develop sulfur-tolerant catalysts. For example, Elliot et al. claimed that the activity of ruthenium catalysts in supercritical water for the catalytic gasification of wet biomass is strongly decreased by the presence of sulfur [43], and Osada et al. found that the adsorption of sulfur on the catalyst was at least partially responsible for the decrease in the process rate for the gasification of lignin [44]. Although sulfur tolerance has been widely investigated, both in the petrochemical and fine chemical industries [45–47], there has been little research into improving sulfur tolerance for catalysts involved in the processing of biomass, such as when using the APR reaction.

Catalysts that combine two metals are common in industrial applications, and often show superior activity, selectivity, and sulfur tolerance compared with their monometallic counterparts [29,48–51]. These improvements might be the result

* Corresponding author.
*E-mail address:* th.maschmeyer@chem.usyd.edu.au (T. Maschmeyer).

0920-5861/$ – see front matter © 2011 Elsevier B.V. All rights reserved.
doi:10.1016/j.cattod.2011.09.014

of electronic perturbations (produced by metal–metal bonding, or by changes in the number of available active sites on the surface of the catalyst) or structural changes leading to more edge-sites, kinks, defects, etc., or smaller particles [51]. Recently, Azad and Duran proposed a mechanism for sulfur poisoning on Pd–Re catalysts for steam reforming of sulfur -laden logistic fuels (diesel, gasoline, jet fuel) [52,53]. They proposed that palladium was able to transfer the sulfur onto the more readily sulfidable rhenium. This 'spillover' of sulfur onto rhenium allows palladium to remain active for longer. Similarly, hydrogen spillover can occur on bimetallic catalysts, and has been reviewed extensively [54,55]. Based on these two spillover phenomena we envisaged the development of a bimetallic catalyst such that one metal would act preferentially as the hydrogenation catalyst and the other would interact preferentially with sulfur-containing compounds. Coupling these functions with hydrogen spillover to the metal-coordinated sulfur species, may enable hydrogen to cleave the sulfur metal bond to effectively regenerate the catalyst.

In the work reported here, platinum was chosen as it displays high activity for the hydrogenation reaction, whereas ruthenium was selected as studies have shown that it possesses a higher affinity for sulfur than does platinum [56]. The acidic, mesoporous SiAlTUD-1 was used as the support material since it is well-established that noble metals immobilised on acidic supports are more sulfur-resistant than they are on other supports [50,57–63]. The mesoporous TUD-1 structure family was chosen because of its characteristic large surface area, high thermostability, and tunable pore sizes.

Common techniques used to synthesise metal nanoparticles include vapour phase techniques [64], sol–gel methods [65], sputtering [66], and co-precipitation [67]. The synthesis of bimetallic nanoparticles is complicated because of the challenges of controlling composition and size distribution [68]. The microemulsion method is an established alternative that can address these problems, and which has been used in the preparation of metal [69,70], metal sulfide [71], and metal halide nanoparticles [72]. The final size of the nanoparticles is controlled by the size of the aqueous droplets, stabilised by the surfactant at the water/oil interface [73]. The size of the droplets are controlled by the water-to-surfactant ratio [68,74].

The hydrogenation of cyclohexene serves as a useful screening reaction because it is very sensitive to sulfur and because hydrogenation reactions are important steps in the conversion of biomass in various processes [75]. Herein, we report the results of studies probing the performance of bimetallic alloy Pt–Ru catalysts as compared to their monometallic counterparts during the hydrogenation of cyclohexene at room temperature in the presence of thiophene as a sulfur poisoning model.

## 2. Materials and methods

### 2.1. Materials

The following reagents were used as received: tetraethylene glycol (TEG), polyethylene glycol dodecyl ether (Brij® 30, $M_n \sim 362$ amu), hydrogen hexachloroplatinate(IV) hydrate ($H_2PtCl_6{\cdot}5H_2O$), decane (all Adrich), aluminium isopropoxide, hydrazine hydrate ($N_2H_4{\cdot}H_2O$) (both Ajax), ruthenium trichloride trihydrate ($RuCl_3{\cdot}3H_2O$) (Strem), n-heptane (APS), cyclohexene (Prolabo), and tetraethylorthosilane (TEOS) (Alfa Aesar). Absolute ethanol (Merck) and acetone (Redox) were analytical grade and were used as received. Deionised water was processed using a Milli-Q (Millipore) Ultrapure Water System. 2-Propanol, purchased from Ajax, was dried over calcium hydride (Aldrich) for 24 h, distilled under $N_2$, and stored under $N_2$ over dried 3 Å molecular sieves. Thiophene (Merck) was purified by passage through neutral alumina.

### 2.2. Catalyst preparation

The SiAlTUD-1 support was prepared using an adaptation of the method described by Simons et al. [76]. Aluminium isopropoxide (6.28 g, 30.7 mmol) was added to a mixture of ethanol (36 mL, 617 mmol), anhydrous 2-propanol (34 mL, 445 mmol), and TEOS (26 mL, 117 mmol) at 45 °C, and the mixture was stirred until all components dissolved. TEG (26 mL, 151 mmol) was added, followed by the dropwise addition of a solution containing ethanol (36 mL, 617 mmol), anhydrous 2-propanol (34 mL, 445 mmol) and water (6 mL, 333 mmol). This mixture was stirred at RT for 30 min, then aged without heating or stirring for 6 h. The resultant white gel was dried at 70 °C for 21 h, then at 98 °C for 2 h after which time the dry material was heated under autogeneous pressure at 165 °C in a Teflon-lined autoclave for 8 h. The template was removed by washing the material in a Soxhlet extractor (Büchi Extraction System (B-811)) using warm ethanol for 3 h. The white solid obtained was dried at 60 °C before being calcined at 600 °C (ramp rate 5 °C $min^{-1}$) for 10 h.

The Pt–Ru, Pt, and Ru nanoparticles were prepared using the water-in-oil microemulsion method [77,78]. Two microemulsions were prepared separately, each containing 80.5% (v/v) n-heptane, 16.5% (v/v) Brij® 30, and 3% (v/v) aqueous phase of either the metal salt precursor solution/s or the reducing agent solution. The aqueous phase of the first microemulsion consisted of either $H_2PtCl_6{\cdot}5H_2O$ solution (0.1 M) or $RuCl_3{\cdot}3H_2O$ solution (0.1 M) or both (each at 0.1 M). The aqueous phase of the second microemulsion consisted of $N_2H_4{\cdot}H_2O$ solution (2.5 M). All the solutions were made using deionised water. The microemulsions were stirred separately for 15 min, before the hydrazine microemulsion was added to the metal salt microemulsion. The combined microemulsion was stirred until the metal cations of the precursors had been reduced to the metals, at which time a colour change occurred and the nanoparticles could be isolated by precipitation with acetone followed by centrifugation (72 h–3 weeks).

The Pt–Ru and Pt on SiAlTUD-1 catalysts, denoted as $Pt_1Ru_{1.5}$ and Pt, respectively (subscripts indicate the relative molar ratios), were prepared by stirring the SiAlTUD-1 with the appropriate nanoparticle suspension. In a typical example, the nanoparticle suspension (89 mL) was added to the support material (700 mg), and the mixture stirred for 24 h. The solid was isolated by centrifugation, washed with warm ethanol for 3 h using the Soxhlet extractor, and dried at 60 °C overnight. The powder was heat-treated at 450 °C (ramp rate 5 °C $min^{-1}$) for 2 h under $N_2$. A Pt/Ru on SiAlTUD-1 mixed monometallic catalyst, denoted as $Pt_1/Ru_1$, was also prepared in the same manner, by combining Pt and Ru nanoparticle suspensions with the support as described above.

The Ru (Ru), Ru–Pt ($Pt_1Ru_3$), and Pt–Ru ($Pt_{1.5}Ru_1$) catalysts could not be reduced as described. In these cases the combined microemulsion solutions were stirred with the support material before the metal salts were reduced. In a typical example, the combined microemulsions (89 mL) were added to the support material (700 mg), and the mixture was stirred for 24 h. The suspension was then centrifuged to isolate the solid, which was washed for 3 h with warm ethanol using the Soxhlet extractor, and dried at 60 °C overnight. The powder was calcined in air at 350 °C (ramp rate 5 °C $min^{-1}$) for 10 h, followed by heat-treatment for 0.5 h under $H_2$.

### 2.3. Characterisation

Powder X-ray diffraction (XRD) measurements were made using a PANalytical X-Pert PRO MRD X-ray diffractometer equipped with a PIXcel detector, and using Ni-filtered $Cu_{K\alpha}$ radiation ($\lambda_{av}$

1.5419 Å). Initial analyses were performed using the PANalytical HighScore software [79]. A Micromeritics ASAP 2020 Accelerated Surface Area and Porosity analyser was used to measure the $N_2$ adsorption/desorption isotherms of the samples at 77 K. Before analysis, samples were degassed at 200 °C. Transmission electron microscopy (TEM) images were recorded digitally with a Gatan slow-scan charge coupled device (CCD) camera on a Philips CM120 Biofilter electron microscope operating at 120 kV. A Varian Vista AX ICP-AES equipped with a CCD detector was used to measure elemental compositions.

### 2.4. Catalytic activity

The hydrogenation reaction was performed in a two-necked, round bottom 50 mL glass Quickfit flask, fitted with Suba-Seal stoppers and equipped with a magnetic stirrer at RT. Cyclohexene (160 μL, 1.58 mmol) and decane (200 μL, 1.03 mmol, internal standard) were added to ethanol (25 mL). The mixture was stirred at a rate of 400 rpm for 5 min in air and a sample (~0.10 mL) was taken. The catalyst (100 mg) was added to the reaction vessel, the mixture was stirred for 10 min, and a sample (~0.10 mL) was taken. The reactor was purged through a cannula with $H_2$ provided from a balloon, filled in-house, to replace the air in the reaction vessel, admitted through a septum cap fitted to one arm of the reactor, and the reaction was run under 1 bar $H_2$ with stirring at 400 rpm for 4 h. Samples (total 8–12, each ~0.10 mL) were taken at regular intervals using a syringe through a septum cap fitted to one arm of the reactor. During sulfur poisoning reactions, thiophene (0.02 μL or 0.20 μL, in 1.0 mL ethanol, equivalent to a thiophene content of 45 ppm or 450 ppm (v/v), or a sulfur content of 57 ppm or 560 ppm (mol/mol) in 160 μL cyclohexene) was added through a septum cap fitted to one arm of the reactor, after admitting $H_2$ to the reactor. All samples taken from the reactor were centrifuged to isolate the catalyst, the supernatant was diluted with ethanol, and the progress of the reaction was analysed using gas chromatography (Shimadzu GC-17A Gas Chromatograph equipped with a BP21 column – 30 m × 0.25 mm I.D.; 0.25 μm film thickness; J & W Scientific - and a flame ionization detector, using Ar as the carrier gas). For catalyst regeneration experiments, the catalyst was isolated from the reaction mixture by centrifugation, and dried in air for use in subsequent reactions. Additionally, for the regeneration reaction with heat treatment, the catalyst was heat-treated under $H_2$ for 1 h at 300 °C (ramp rate 5 °C $min^{-1}$).

### 2.5. Normalisation

As the TEM micrographs and bulk XRD patterns indicated similar metal particle sizes across the catalyst batches, it was assumed that the metal dispersion was relatively equal across all samples. Therefore, the catalytic results were calculated as turn-over-frequencies (TOF) from the number of moles of product (cyclohexane) at 10% conversion, and then normalised per mole of platinum (as determined by ICP-AES) per unit time (using the formula TOF = [mol cyclohexane]/[mol Pt] × time). It should be noted that in all cases the mass balance was >90%.

## 3. Results and discussion

### 3.1. Characterisation

The acidic, mesoporous, aluminosilicate SiAlTUD-1 used as the catalyst support, was synthesised according to the literature [76]. Its BET surface area of 587 $m^2 g^{-1}$, total pore volume of 1.1 $cm^3 g^{-1}$, and maximum pore size of 15 nm are in close agreement with the literature values of ~600 $m^2 g^{-1}$, 1.1 $cm^3 g^{-1}$, and 15 nm, respectively [76]. Analysis of the product using ICP-AES gave the silicon to aluminium ratio (Si:Al) as 4.4:1, consistent with the 5:1 composition of the starting gel mixture.

The following six catalysts were prepared using this support material, i.e. in addition to a pure ruthenium (Ru) and a pure platinum (Pt) catalyst, a mixed monometallic catalyst ($Pt_1/Ru_1$) was prepared by first separately reducing the platinum and ruthenium monometallic precursor solutions and subsequently mixing the resulting suspensions in the immobilisation step. Three bimetallic alloyed catalysts ($Pt_1Ru_3$, $Pt_1Ru_{1.5}$, and $Pt_{1.5}Ru_1$) with different ruthenium and platinum ratios were also prepared. As outlined in Section 2, not all catalysts could be directly reduced in the water-in-oil microemulsion, therefore two different strategies were followed to reduce and immobilise the metal nanoparticles onto the support material. The first group of catalysts consists of $Pt_1Ru_{1.5}$, Pt, and $Pt_1/Ru_1$, which were directly reduced with hydrazine in the water-in-oil microemulsion and immobilised onto the support, followed by a heat treatment under nitrogen to remove all organic material. The second group consists of Ru, $Pt_1Ru_3$, and $Pt_{1.5}Ru_1$. For these catalysts it was necessary to immobilise the metal precursors in a first step by impregnation from solution, followed by calcination and subsequent hydrogenation. The physical properties of all catalysts are presented in Table 1.

The Pt to Ru ratios for the bimetallic alloyed catalysts, determined by ICP-AES (Table 1), cover a broad range from 1:1.6 for $Pt_1Ru_{1.5}$ to 1:2.6 for $Pt_1Ru_3$ to 1.4:1 for $Pt_{1.5}Ru_1$, and the mixed monometallic $Pt_1/Ru_1$ catalyst exhibits a metal ratio of 1:1. All metal ratios are in good agreement with those expected from the concentrations of the starting precursor solutions. Nitrogen sorption measurements of the catalysts, listed in Table 1, indicate a general decrease in surface areas and pore volumes compared with the unmodified support material. The surface areas and pore volumes were calculated to be between 390 to 500 $m^2 g^{-1}$ and 0.9 to 1.1 $cm^3 g^{-1}$, respectively. The decrease in the surface area of the material compared to that of the pure silica can be attributed to the heat treatment of the support material during the immobilisation step and to the immobilisation itself [80]. A general trend is not apparent between metal loading and surface areas. As expected, the pore size of silica is not affected by the immobilisation process.

As shown in Fig. 1a, the XRD patterns of all samples display the typical reflections for platinum or ruthenium, indicating the presence of the metal nanoparticles, and in the case of the bimetallic samples, the formation of a Pt–Ru or Ru–Pt alloy. All supported nanoparticles have retained small particle sizes, generally below 15 nm, except $Pt_{1.5}Ru_1$, which has a particle size of 20 nm, as determined using the Scherrer equation. It can be deduced from the XRD pattern that the sample $Pt_1Ru_3$ exhibits the hcp crystal structure characteristic of ruthenium which is also observed in the pure catalyst Ru, which, for the $Pt_1Ru_3$ sample, is consistent with its high ruthenium content (Pt to Ru ratio of 1:2.6). However, extrapolating from the Pt–Ru equilibrium phase diagram of bulk ruthenium and platinum (reported only for $T \geq 500$ °C) [81], reflections attributable to the fcc phase of platinum might also be expected to be observed in the XRD pattern in the present case as in this range both metals are immiscible (at least at $T \geq 500$ °C) [82,83]. Although a second phase could not be detected in the XRD pattern, the intensities of the reflections observed are relatively weak and broad due to the nature of the supported nanoparticles. In the literature different observations have been reported, for instance, Chu et al. could detect both phases in the XRD data of ca. 13 nm Pt–Ru nanoparticles with the same metal ratio [84]. In contrast, Pan et al. published results of alloyed Pt–Ru nanoparticles, again with the same metal ratio, where only a twinned fcc structure could be detected indicating the threshold between the fcc and hcp structures [85].

When the platinum content is slightly increased as in catalyst $Pt_1Ru_{1.5}$, the catalyst exhibits the fcc crystal structure

**Table 1**
Physical properties of the unloaded support and all catalysts.

| Catalyst | Metal[a] (wt.%) | Pt (mol.%) | Ru (mol.%) | $a$ (Å) | $\sigma$ (Å) | $S_{BET}$ ($m^2\,g^{-1}$) | $V_{Pore}$ ($cm^3\,g^{-1}$) |
|---|---|---|---|---|---|---|---|
| SiAlTUD-1 | 0 | – | – | – | – | 587 | 1.10 |
| Ru[b] | 0.50 | 0 | 100 | 2.7098 | 0.0005 | 437 | 1.03 |
| $Pt_1Ru_3$[c] | 0.06 | 28 | 72 | 2.7133 | 0.0016 | 451 | 1.00 |
| $Pt_1Ru_{1.5}$[b] | 0.20 | 38 | 62 | 3.8905 | 0.0005 | 497 | 1.11 |
| $Pt_{1.5}Ru_1$[b] | 0.10 | 59 | 41 | 3.9178 | 0.0001 | 399 | 0.90 |
| Pt[c] | 1.79 | 100 | 0 | 3.9199 | 0.0001 | 455 | 0.91 |
| $Pt_1/Ru_1$[c] | 1.73 | 49 | 51 | 3.9153 | 0.0001 | 388 | 0.95 |

[a] Total metal loading.
[b] Immobilised followed by reduction with hydrogen.
[c] Reduced with hydrazine followed by immobilisation.

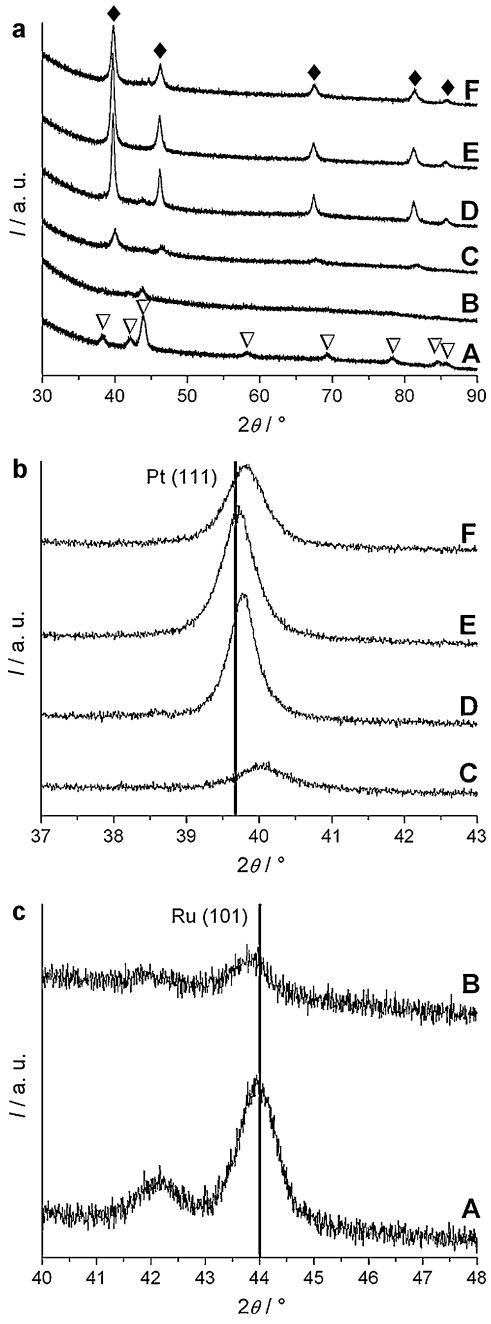


**Fig. 1.** XRD patterns (a) of all catalysts, (b) in the range of 37–43 2$\theta$ showing the (1 1 1) reflection of platinum and (c) in the range of 40–48 2$\theta$ showing the (1 0 1) reflection of ruthenium with (A) Ru, (B) $Pt_1Ru_3$, (C) $Pt_1Ru_{1.5}$, (D) $Pt_{1.5}Ru_1$, (E) Pt and (F) $Pt_1/Ru_1$. Patterns of references are JCPDS 00-001-1190 for platinum (♦) and JCPDS 00-006-663 for ruthenium (▽) [86,87].

characteristic of platinum, rather than the hcp crystal structure of ruthenium, which is in good agreement with the literature [82,83,88]. The XRD patterns of catalyst $Pt_{1.5}Ru_1$ and the pure catalyst Pt show the typical platinum patterns, as expected due to their high platinum content. However, due to a small reflection at 44 degrees in 2$\theta$ in the XRD pattern of catalyst $Pt_{1.5}Ru_1$, the presence of an additional minor Ru phase cannot be completely excluded. In the case of the mixed monometallic catalyst $Pt_1/Ru_1$, in which the two separately reduced monometallic platinum and ruthenium suspensions were mixed prior to the immobilisation, the resulting XRD pattern reveals mainly the Pt reflections. Nevertheless, reflections of the ruthenium phase can also be found, indicating its presence.

To evaluate the bimetallic character of these catalysts, the (1 1 1) reflection of platinum (Fig. 1b) and the (1 0 1) of ruthenium (Fig. 1c) were analysed. In Fig. 1b it is obvious that with increasing ruthenium content ($Pt < Pt_{1.5}Ru_1 < Pt_1Ru_{1.5}$) the (1 1 1) reflection shifts to higher 2$\theta$ values. Thus, the lattice constants for these catalysts decrease from 3.9199 Å for pure platinum in catalyst Pt to 3.9178 Å for $Pt_{1.5}Ru_1$ and down to 3.8905 Å for $Pt_1Ru_{1.5}$ (Table 1). This result reflects the fact that more ruthenium, which has a smaller atomic radius than platinum ($r_{Ru}$ = 1.34 Å vs $r_{Pt}$ = 1.38 Å), is being incorporated in the platinum lattice, and is consistent with alloy formation. Interestingly, catalyst $Pt_1/Ru_1$ also shows a small shift to higher 2$\theta$ values, displaying a lattice constant of 3.9153 Å. This smaller lattice constant indicates a slightly alloyed character, which might arise during the final heat treatment. However, as the shift to lower 2$\theta$ is only slight, in spite of the relatively high ruthenium content, it is likely that most of the ruthenium does, indeed, exist in a separate phase. In the case of catalyst $Pt_1Ru_3$, a small but obvious shift towards smaller 2$\theta$ values is observed, which indicates the incorporation of the larger platinum into the ruthenium lattice. The lattice constants were calculated to be 2.7098 Å for the pure Ru catalyst and to be 2.7133 Å for $Pt_1Ru_3$. This result, in combination with the lack of a second phase, indicates at least partial alloy formation, which is contrary to the phase diagram of the bulk materials but in agreement with the work of Pan et al. However, due to the nature of the XRD data set a second platinum phase cannot be completely excluded. All other XRD results of the bimetallic alloyed catalysts are in good agreement with the trends observed in studies of Pt–Ru and Ru–Pt alloys with various compositions [82,84,89].

The TEM micrographs of the catalysts, presented in Fig. 2, reveal a good dispersion of the nanoparticles on the surface of the supports. It is apparent that the nanoparticles have retained their spherical shape, dispersion and a narrow size distribution (12–15 nm). The main exception, $Pt_{1.5}Ru_1$ (Fig. 2d), has a slightly larger particle size of approximately 20 nm, which is in good agreement with the size obtained from the XRD analysis.

### 3.2. Catalytic activity

The turn-over-frequencies (TOF) were determined at 10% conversion to minimise distortions due to batch conditions and

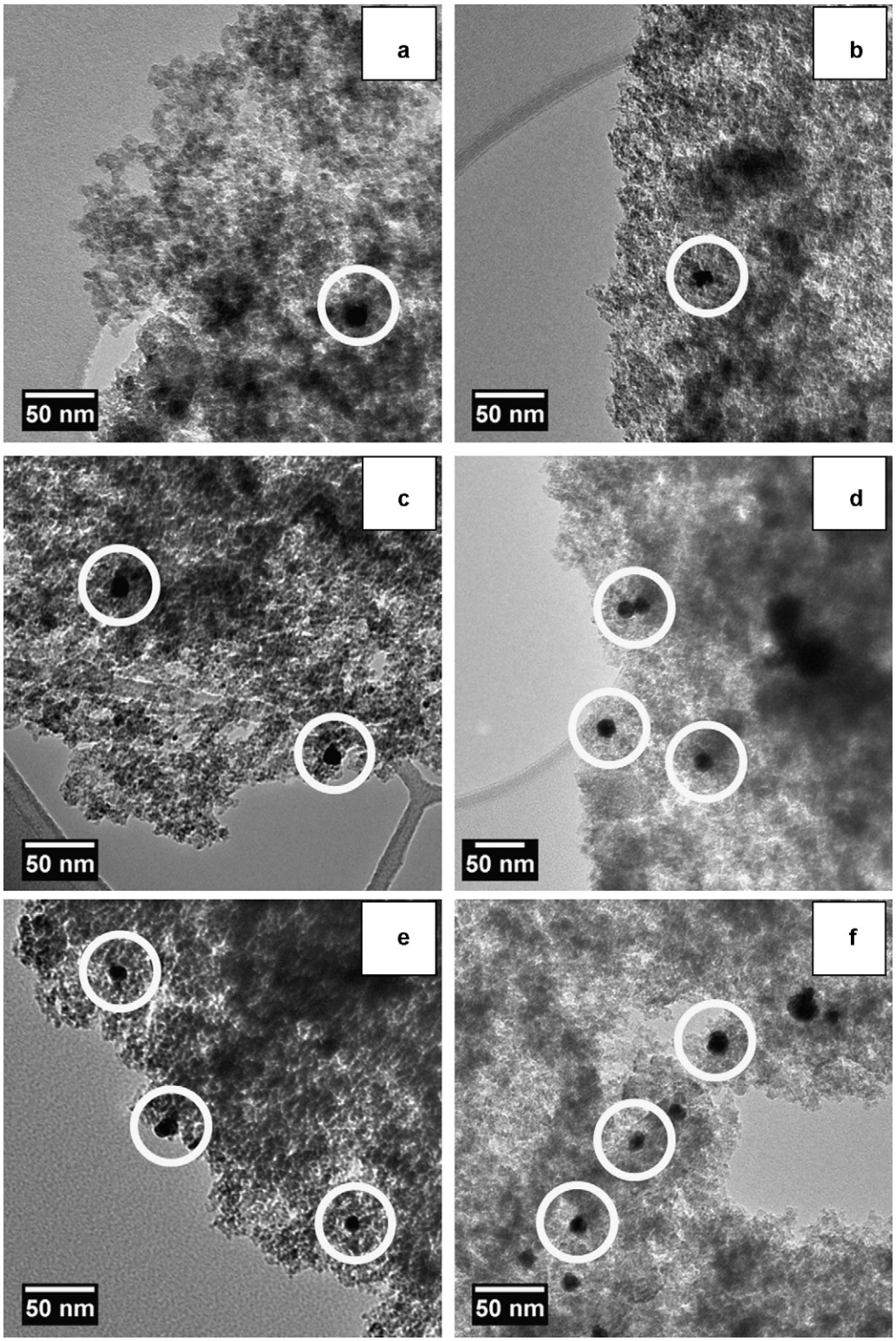


**Fig. 2.** TEM micrographs of the catalysts prepared: (a) Ru, (b) $Pt_1Ru_3$, (c) $Pt_1Ru_{1.5}$, (d) $Pt_{1.5}Ru_1$, (e) Pt and (f) $Pt_1/Ru_1$. The nanoparticles are highlighted with white circles.

variance of metal loading between catalysts. They are summarized in Table 2. All alloy catalysts exhibit higher activity than the non-alloyed catalysts. Ruthenium alloys are more sulfur tolerant than pure platinum or a mixture of supported platinum/ruthenium nanoparticles. Ruthenium on its own is not active. At 57 ppm of added sulfur there appears to be a trend that shows the greater the ruthenium component of the alloy the greater its sulfur tolerance. However, at low activity in the presence of 560 ppm sulfur this trend becomes less clear.

The close to linear conversion with time (Fig. 3) for the alloys as compared to pure platinum are consistent with a hydrogen/sulfur spillover equilibrium having been established. The study of the alloyed catalysts reveals that the platinum to ruthenium ratio plays

**Table 2**
TOF results of the hydrogenation of cyclohexene in ethanol at RT under 1 bar $H_2$.

| Catalyst | TOF ($s^{-1}$ [c]) | | |
|---|---|---|---|
| | 0 ppm S[g] | 57 ppm S[g] | 560 ppm S[g] |
| Ru[a,d] | 0 | 0 | 0 |
| $Pt_1Ru_3$[a] | 63.3 | 9.8 | 1.8 |
| $Pt_1Ru_{1.5}$[b] | 23.0 | 8.9 | 3.3 |
| $Pt_1Ru_{1.5}$[e] | 24.9 | – | – |
| $Pt_1Ru_{1.5}$[f] | 4.7 | – | – |
| $Pt_{1.5}Ru_1$[a] | 34.7 | 6.4 | 2.3 |
| Pt[b] | 1.4 | 0.3 | 0 |
| $Pt_1/Ru_1$[b] | 1.9 | 0.4 | 0 |

[a] Immobilised followed by reduction with hydrogen.
[b] Reduced with hydrazine followed by immobilisation.
[c] At 10% conversion, TOF = [mol cyclohexane]/[mol Pt] × time.
[d] Catalyst was completely inactive for the reaction studied.
[e] After exposing to 560 ppm S, recycling and reduction under hydrogen.
[f] After exposing to 560 ppm S, recycling and drying in air at RT.
[g] Equals a proportion of 45 ppm or 450 ppm thiophene in 160 μL cyclohexene.

a crucial role for the catalytic performance and needs further investigations.

To determine the influence of sulfur poisoning on the alloy character of the bimetallic catalysts, the Pt(1 1 1) reflection in the case of $Pt_{1.5}Ru_1$ and $Pt_1Ru_{1.5}$ and the Ru(1 0 1) reflection for $Pt_{1.5}Ru_1$ of the XRD powder patterns were monitored before and after the catalytic reaction with 560 ppm sulfur (Figs. 4 and 5). This comparison involves the catalyst having been isolated from the thiophene-containing solution after the flow of hydrogen was stopped. Fig. 4 (A and B) illustrates that after poisoning $Pt_1Ru_{1.5}$ with 560 ppm sulfur the Pt(1 1 1) reflection shifts towards lower $2\theta$. This shift indicates that the catalyst loses some of its alloy character, partially separating into two metal domains, and the lattice constant

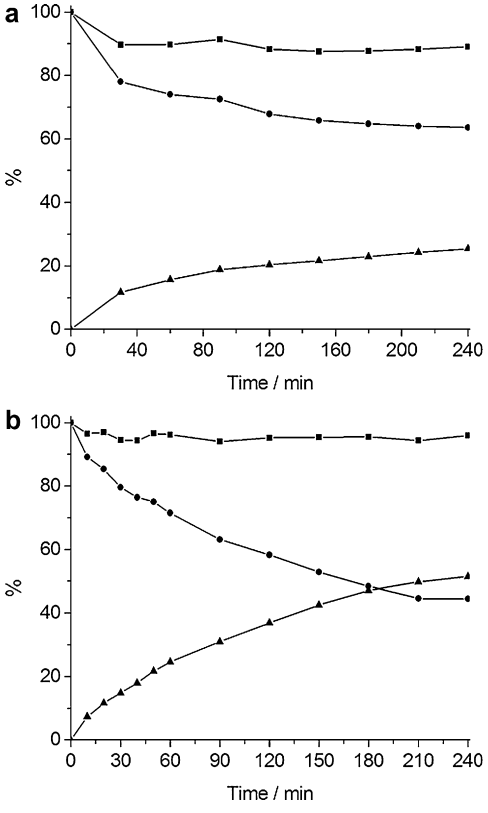


**Fig. 3.** Plot of cyclohexene conversion (●), formation of cyclohexane (▲), and mass balance (■) (a) in the presence of 560 ppm sulfur and (b) in the presence of 0 ppm sulfur but after being exposed to 560 ppm sulfur, isolated and re-used (without being re-conditioned by heat treatment under hydrogen) for catalyst $Pt_1Ru_{1.5}$.

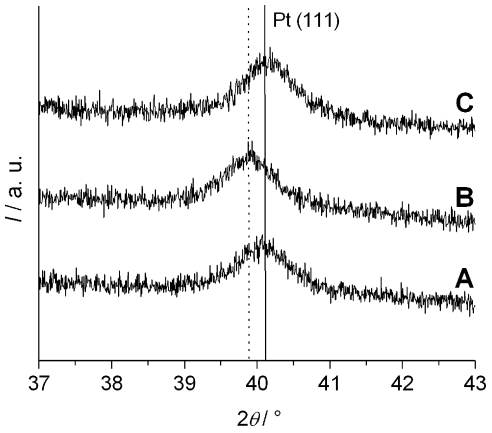


**Fig. 4.** XRD patterns of $Pt_1Ru_{1.5}$ catalyst (A) before sulfur poisoning, (B) after sulfur poisoning with 560 ppm sulfur and (C) after regeneration with heat treatment under $H_2$. The solid line indicates the reflection position in the absence of sulfur and the dotted line, that in the presence of sulfur.

increases accordingly to 3.9060 Å. This value is between the lattice constant of the catalyst before poisoning (3.8905 Å) and the lattice constant of pure platinum (3.9199 Å) [89]. This result suggests that the ruthenium has been sequestered in the presence of thiophene, maybe in the form of ruthenium sulfide or a ruthenium–thiophene complex. The coordination of sulfur to ruthenium would lead to an internal restructuring of the particle, which suggests that ruthenium is acting as a sulfur trap. The observed shift of the reflections in the XRD patterns is consistent with studies by Menegazzo et al., who observed similar shifts, in their investigations of sulfur

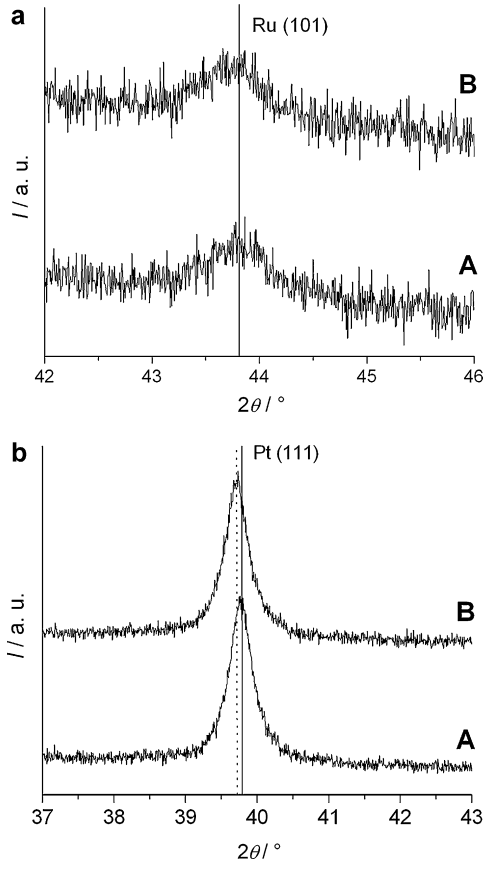


**Fig. 5.** XRD patterns of (a) $Pt_1Ru_3$ and (b) $Pt_{1.5}Ru_1$ (A) before and (B) after sulfur poisoning with 560 ppm sulfur. The solid line indicates the reflection position in the absence of sulfur and the dotted line in the presence of sulfur.

poisoning on Pd–Au catalysts [90]. They attributed the shift to the formation of palladium sulfide, which could be confirmed by the presence of an additional palladium sulfide reflection, although no additional reflections could be observed in the present case. However, Menegazzo et al. used sodium sulfide (not thiophene) as sulfur source to poison the catalyst. It should be noted that this shift cannot be observed when 57 ppm sulfur is used to poison the catalyst.

To test if the sulfur poisoning and Pt–Ru alloy internal restructuring is reversible, a $Pt_1Ru_{1.5}$ catalyst, previously operated in the presence of 560 ppm sulfur, was heat-treated under hydrogen for 1 h at 300 °C. Upon heat treatment, the XRD powder pattern (C in Fig. 4) shows that the reflection has shifted back towards higher $2\theta$ and the lattice constant (3.8891 Å) has almost reached is former value. This observation would be consistent with the catalyst returning to its original Pt–Ru alloy form, suggesting that the sulfur is no longer coordinated to the ruthenium, which has been incorporated back into the platinum lattice. Hence, there appears to be a dynamic alloy/de-alloying process occurring during the poisoning and regeneration processes. To verify that the catalyst was indeed regenerated, it was subsequently tested for its hydrogenation activity in the absence of sulfur, yielding a TOF of 24.9 $s^{-1}$, which is comparable to the TOF before poisoning (TOF of 23.0 $s^{-1}$, Table 2). This reversibility is consistent with the suggestion made above as to the occurrence of hydrogen/sulfur spillover in situ explaining the sulfur tolerance of the alloy catalyst to some degree. To underpin this suggestion, in an additional experiment the $Pt_1Ru_{1.5}$ catalyst, again exposed to 560 ppm sulfur, was isolated and re-used in a subsequent hydrogenation reaction in the absence of added thiophene, but this time without being re-conditioned by heat treatment under hydrogen. The catalyst yielded a TOF of 4.7 $s^{-1}$ which is higher than the TOF achieved in the presence of 560 ppm sulfur (TOF of 3.3 $s^{-1}$, Table 2), as shown in Fig. 3a and b. If the sulfur species had been adsorbed irreversibly on the catalyst surface, no subsequent improvement in the activity of the catalyst would have been observable. However, as the catalyst did regain some activity, this result suggests that the sulfur poisoning is a dynamic and reversible process. The precise fate of the thiophene (simple equilibrium or conversion into eventually $H_2S$) will be elucidated with further experiments using very precise vibrational spectroscopic techniques that can deal with the very low surface coverages. However, under the relatively mild screening conditions used here, one would not assume full decomposition to $H_2S$, and we found no evidence of this gas being present.

In the case of $Pt_1Ru_3$ no observable shift could be found (Fig. 5a), despite it being severely poisoned. This lack of shift could be attributed to the high content of ruthenium in $Pt_1Ru_3$ that results in the hcp crystal structure, making the segregation of ruthenium out of the alloy impossible to observe. Contrarily, in the XRD patterns of $Pt_{1.5}Ru_1$ (Fig. 5b), a slight shift towards lower $2\theta$ is observed. This XRD result indicates the internal restructuring of the Pt–Ru alloy, similar to the restructuring observed for $Pt_1Ru_{1.5}$, although the shift towards the (1 1 1) reflection of pure platinum is less pronounced for $Pt_{1.5}Ru_1$ than for $Pt_1Ru_{1.5}$. A reason can be that $Pt_{1.5}Ru_1$ had a much higher relative platinum content (Table 1) and therefore a smaller initial shift after the incorporation of the ruthenium into the lattice than $Pt_1Ru_{1.5}$. Whereas the lattice constant of $Pt_1Ru_{1.5}$ after poisoning is 3.9060 Å, indicating a partial separation of the alloy into metal domains, the lattice constant of $Pt_{1.5}Ru_1$ after poisoning is 3.9214 Å (c.f. the lattice constant of platinum of 3.9199 Å). Thus, the XRD pattern after poisoning suggests that $Pt_{1.5}Ru_1$ no longer displays any alloyed character, and the Pt–Ru appears to have completely separated into two metal domains, limiting the events of hydrogen and/or sulfur spillovers.

In combination with the catalysis results there appears to be a correlation between the presence of an alloy character after poisoning with sulfur and the activity of the catalysts. The catalyst that is least poisoned ($Pt_1Ru_{1.5}$) exhibits only partial alloy separation, whereas the catalyst which displays greater overall poisoning ($Pt_{1.5}Ru_1$) exhibits complete alloy separation.

## 4. Conclusion

Improved sulfur tolerance in the catalysis of cyclohexene hydrogenation is observed for catalysts consisting of bimetallic Pt–Ru nanoparticles supported on a high surface area mesoporous Si/Al support of the TUD-1 type. This sulfur tolerance, observed for certain Ru to Pt ratios, might be due to sulfur and hydrogen intraparticle spillover. Regeneration of sulfur poisoned catalysts by heating in hydrogen after the reaction has been demonstrated. This is consistent with the operation of an in situ self regeneration process during the reaction. To get a better understanding of the (self-) regeneration processes in situ EXAFS studies are being pursued.

## References

[1] J.N. Chheda, G.W. Huber, J.A. Dumesic, Angew. Chem. Int. Ed. 46 (2007) 7164–7183.
[2] D.L. Klass, Biomass for Renewable Energy, Fuels, and Chemicals, Academic Press, San Diego, 1998.
[3] L.R. Lynd, C.E. Wyman, T.U. Gerngross, Biotechnol. Prog. 15 (1999) 777–793.
[4] G.W. Huber, S. Iborra, A. Corma, Chem. Rev. 106 (2006) 4044–4098.
[5] L.D. Schmidt, P.J. Dauenhauer, Nature 447 (2007) 914–915.
[6] A. Demirbas, Prog. Energy Combust. 33 (2007) 1–18.
[7] G.W. Huber, J.A. Dumesic, Catal. Today 111 (2006) 119–132.
[8] R.W.R. Zwart, H. Boerrigter, Energy Fuel 19 (2005) 591–597.
[9] N.Y. Chen, T.F. Degnan Jr., L.R. Koenig, Chem. Tech. 16 (1986) 506–511.
[10] C. Rioche, S. Kulkarni, F.C. Meunier, J.P. Breen, R. Burch, Appl. Catal. B-Environ. 61 (2005) 130–139.
[11] D.C. Elliott, D. Beckman, A.V. Bridgwater, J.P. Diebold, S.B. Gevert, Y. Solantausta, Energy Fuel 5 (1991) 399–410.
[12] D.C. Elliott, Energy Fuel 21 (2007) 1792–1815.
[13] R. Katzen, G.T. Tsao, Adv. Biochem. Eng. Biotechnol. 70 (2000) 77–91.
[14] R.R. Davda, J.W. Shabaker, G.W. Huber, R.D. Cortright, J.A. Dumesic, Appl. Catal. B-Environ. 56 (2005) 171–186.
[15] M. Osada, T. Sato, M. Watanabe, M. Shirai, K. Arai, Combust. Sci. Technol. 178 (2006) 537–552.
[16] Y. Matsumura, M. Sasaki, K. Okuda, S. Takami, S. Ohara, M. Umetsu, T. Adschiri, Combust. Sci. Technol. 178 (2006) 509–536.
[17] M. Osada, O. Sato, M. Watanabe, K. Arai, M. Shirai, Energy Fuel 20 (2006) 930–935.
[18] T. Yoshida, Y. Oshima, Ind. Eng. Chem. Res. 43 (2004) 4097–4104.
[19] T. Sato, M. Osada, M. Watanabe, M. Shirai, K. Arai, Ind. Eng. Chem. Res. 42 (2003) 4277–4282.
[20] M. Osada, T. Sato, M. Watanabe, T. Adschiri, K. Arai, Energy Fuel 18 (2004) 327–333.
[21] D. Wang, D. Montane, E. Chornet, Appl. Catal. A-Gen. 143 (1996) 245–270.
[22] D. Wang, S. Czernik, D. Montane, M. Mann, E. Chornet, Ind. Eng. Chem. Res. 36 (1997) 1507–1518.
[23] D. Wang, S. Czernik, E. Chornet, Energy Fuel 12 (1998) 19–24.
[24] M. Marquevich, S. Czernik, E. Chornet, D. Montane, Energy Fuel 13 (1999) 1160–1166.
[25] L. Garcia, R. French, S. Czernik, E. Chornet, Appl. Catal. A-Gen. 201 (2000) 225–239.
[26] S. Czernik, R. French, C. Feik, E. Chornet, Ind. Eng. Chem. Res. 41 (2002) 4209–4215.
[27] J.W. Shabaker, G.W. Huber, J.A. Dumesic, J. Catal. 222 (2004) 180–191.
[28] J.W. Shabaker, R.R. Davda, G.W. Huber, R.D. Cortright, J.A. Dumesic, J. Catal. 215 (2003) 344–352.
[29] G.W. Huber, J.W. Shabaker, S.T. Evans, J.A. Dumesic, Appl. Catal. B-Environ. 62 (2006) 226–235.
[30] G.W. Huber, J.W. Shabaker, J.A. Dumesic, Science 300 (2003) 2075–2078.
[31] R.R. Davda, J.W. Shabaker, G.W. Huber, R.D. Cortright, J.A. Dumesic, Appl. Catal. B-Environ. 43 (2003) 13–26.
[32] R.R. Davda, J.A. Dumesic, Chem. Commun. (2004) 36–37.
[33] R.D. Cortright, R.R. Davda, J.A. Dumesic, Nature 418 (2002) 964–967.
[34] Y.-C. Lin, G.W. Huber, Energy Environ. Sci. 2 (2009) 68–80.
[35] G.W. Huber, R.D. Cortright, J.A. Dumesic, Angew. Chem. Int. Ed. 43 (2004) 1549–1551.
[36] R.M. West, Z.Y. Liu, M. Peter, C.A. Gartner, J.A. Dumesic, J. Mol. Catal. A-Chem. 296 (2008) 18–27.
[37] R.M. West, Z.Y. Liu, M. Peter, J.A. Dumesic, ChemSusChem 1 (2008) 417–424.
[38] G.W. Huber, J.N. Chheda, C.J. Barrett, J.A. Dumesic, Science 308 (2005) 1446–1450.
[39] N. Yan, C. Zhao, P.J. Dyson, C. Wang, L.-t. Liu, Y. Kou, ChemSusChem 1 (2008) 626–629.

[40] E.L. Kunkes, D.A. Simonetti, R.M. West, J.C. Serrano-Ruiz, C.A. Gaertner, J.A. Dumesic, Science 322 (2008) 417–421.
[41] J.N. Chheda, J.A. Dumesic, Catal. Today 123 (2007) 59–70.
[42] J.M. Robinson, S.R. Barrett, K. Nhoy, R.K. Pandey, J. Phillips, O.A. Ramirez, R.I. Rodriguez, Energy Fuel 23 (2009) 2235–2241.
[43] D.C. Elliott, G.G. Neuenschwander, T.R. Hart, R.S. Butner, A.H. Zacher, M.H. Engelhard, J.S. Young, D.E. McCready, Ind. Eng. Chem. Res. 43 (2004) 1999–2004.
[44] M. Osada, N. Hiyoshi, O. Sato, K. Arai, M. Shirai, Energy Fuel 21 (2007) 1400–1405.
[45] C.H. Bartholomew, P.K. Agrawal, J.R. Katzer, Adv. Catal. 31 (1982) 135–242.
[46] J.A. Rodriguez, Prog. Surf. Sci. 81 (2006) 141–189.
[47] E. Kullavanijaya, N.W. Cant, D.L. Trimm, Catal. Lett. 75 (2001) 25–29.
[48] J.A. Rodriguez, D.W. Goodman, Surf. Sci. Rep. 14 (1991) 1–107.
[49] G.A. Somorjai, Introduction to Surface Chemistry and Catalysis, Wiley, New York, 1994.
[50] H. Yasuda, Y. Yoshimura, Catal. Lett. 46 (1997) 43–48.
[51] J.A. Rodriguez, J. Hrbek, Acc. Chem. Res. 32 (1999) 719–728.
[52] A.-M. Azad, M.J. Duran, Appl. Catal. A-Gen. 330 (2007) 77–88.
[53] A.-M. Azad, D. Sundararajan, Adv. Mater. Sci. Eng. 325683 (2010) 325612 pp.
[54] W.C. Conner Jr., J.L. Falconer, Chem. Rev. 95 (1995) 759–788.
[55] F. Roessner, Spillover effects, in: Handbook of Heterogeneous Catalysis, 2nd ed., Wiley-VCH Verlag GmbH & Co. KGaA, 2008, pp. 1574–1585.
[56] H. Wise, Mechanisms of catalyst poisoning by sulfur species, in: C.H. Bartholomew, J.B. Butt (Eds.), Catalyst Deactivation Proceedings of the 5th International Symposium, Elsevier Science Publishers, Amsterdam, 1991, pp. 497–503.
[57] R. Frety, P.N. Da Silva, M. Guenin, Catal. Lett. 3 (1989) 9–16.
[58] R. Frety, P.N. Da Silva, M. Guenin, Appl. Catal. 57 (1990) 99–103.
[59] P. Marécot, J.R. Mahoungou, J. Barbier, Appl. Catal. A-Gen. 101 (1993) 143–149.
[60] L.J. Hoyos, M. Primet, H. Praliaud, J. Chem. Soc. Faraday Trans. 88 (1992) 113–119.
[61] A. Stanislaus, B.H. Cooper, Catal. Rev. 36 (1994) 75–123.
[62] B.H. Cooper, B.B.L. Donnis, Appl. Catal. A-Gen. 137 (1996) 203–223.
[63] W.M.H. Sachtler, A.Y. Stakheev, Catal. Today 12 (1992) 283–295.
[64] R.W. Siegel, S. Ramasamy, H. Hahn, Z. Li, T. Lu, R. Gronsky, J. Mater. Res. 3 (1988) 1367–1372.
[65] B. Fegley Jr., P. White, H.K. Bowen, Am. Ceram. Soc. Bull. 64 (1985) 1115–1120.
[66] P. Fayet, L. Woeste, Z. Phys. D Atoms Mol. Cl. 3 (1986) 177–182.
[67] Z.X. Tang, C.M. Sorensen, K.J. Klabunde, G.C. Hadjipanayis, J. Colloid Interface Sci. 146 (1991) 38–52.
[68] X. Zhang, K.Y. Chan, Chem. Mater. 15 (2003) 451–459.
[69] M. Boutonnet, J. Kizling, P. Stenius, G. Maire, Colloids Surf. 5 (1982) 209–225.
[70] D.-H. Chen, S.-H. Wu, Chem. Mater. 12 (2000) 1354–1360.
[71] A.R. Kortan, R. Hull, R.L. Opila, M.G. Bawendi, M.L. Steigerwald, P.J. Carroll, L.E. Brus, J. Am. Chem. Soc. 112 (1990) 1327–1332.
[72] V. Pillai, P. Kumar, M.S. Multani, D.O. Shah, Colloids Surf. A 80 (1993) 69–75.
[73] I. Capek, Adv. Colloid Interface 110 (2004) 49–74.
[74] S. Eriksson, U. Nylén, S. Rojas, M. Boutonnet, Appl. Catal. A-Gen. 265 (2004) 207–219.
[75] C. Zhao, Y. Kou, A.A. Lemonidou, X.B. Li, J.A. Lercher, Angew. Chem. Int. Ed. 48 (2009) 3987–3990.
[76] C. Simons, U. Hanefeld, I.W.C.E. Arends, R.A. Sheldon, T. Maschmeyer, Chem. Eur. J. 10 (2004) 5829–5835.
[77] L.G.R.A. Santos, C.H.F. Oliveira, I.R. Moraes, E.A. Ticianelli, J. Electroanal. Chem. 596 (2006) 141–148.
[78] G. Siné, C. Comninellis, Electrochim. Acta 50 (2005) 2249–2254.
[79] PANalytical, PANalytical HighScore Almelo, The Netherlands, 2010.
[80] I.C. Neves, G. Botelho, A.V. Machado, P. Rebelo, S. Ramoa, M.F.R. Pereira, A. Ramanathan, P. Pescarmona, Polym. Degradr. Stabil. 92 (2007) 1513–1519.
[81] H. Okamoto, J. Phase Equilib. Diffus. 29 (2008) 471.
[82] H.A. Gasteiger, P.N. Ross Jr., E.J. Cairns, Surf. Sci. 293 (1993) 67–80.
[83] R.M. Todi, A.P. Warren, K.B. Sundaram, K. Barmak, K.R. Coffey, IEEE Electron Device Lett. 27 (2006) 542–545.
[84] D. Chu, S. Gilman, J. Electrochem. Soc. 143 (1996) 1685–1690.
[85] C. Pan, F. Dassenoy, M.J. Casanove, K. Philippot, C. Amiens, P. Lecante, A. Mosset, B. Chaudret, J. Phys. Chem. B 103 (1999) 10098–10101.
[86] H.E. Swanson, E. Tatge, Natl. Bur. Stand. Circ. (US) 539 (1953) 95pp.
[87] H.E. Swanson, N.T. Gilfrich, G.M. Ugrinic, Natl. Bur. Stand. Circ. (US) 5 (1955) 75pp.
[88] C. Hamel, S. Garbarino, E. Irissou, M.-P. Bichat, D. Guay, J. Phys. Chem. C 114 (2010) 18931–18939.
[89] E. Antolini, F. Cardellini, J. Alloy Compd. 315 (2001) 118–122.
[90] F. Menegazzo, P. Canton, F. Pinna, N. Pernicone, Catal. Commun. 9 (2008) 2353–2356.